GPS Solutions (2020) 24:27
https://doi.org/10.1007/s10291-019-0933-0

ORIGINAL ARTICLE

Apparent clock and TGD biases between BDS-2 and BDS-3

Yize Zhang[1,2] · Nobuaki Kubo[1] · Junping Chen[2,3] · Feng-Yu Chu[1] · Ahao Wang[3,4] · Jiexian Wang[4]

Received: 4 July 2019 / Accepted: 13 November 2019

Abstract
With the official commencement of the BDS-3 service, the BeiDou navigation satellite system (BDS) has become a global navigation satellite system. The characteristics of the new BDS-3 satellites, including code bias, are worth investigating. An apparent pair of clock and timing group delay (TGD) biases between BDS-2 and BDS-3 are found when assessing the BDS signal-in-space range error (SISRE) with 5-months of data spanning day of year (DOY) 6 to 145 in 2019, which results from the system bias between the broadcast ephemeris and the precise products provided by Wuhan University and the Chinese Academy of Science. The biases of the broadcast ephemeris are therefore calibrated when aligning to precise products. When these biases are corrected, the overall performance of the BDS SISRE decreases from 1.41 to 0.84 m for the B1I/B3I frequency. To further investigate the biases, we analyze 68 multi-GNSS experiment stations equipped with different receivers based on raw pseudorange measurements. It is found that the clock bias seems similar at each receiver, while the TGD bias from B3I to B1I depends on receiver type, with a value of −0.48, −0.98, and −1.60 m for Javad, Trimble, and Septentrio receiver, respectively. The estimated average clock and TGD biases show good agreement with that from broadcast ephemeris and precise product comparison. When the calibrated clock and TGD biases are corrected in the BDS-3 satellites, the SPP performance improves from 0.3 to 31.8%, depending on frequency and receiver type. For real-time kinematic positioning, when the clock and TGD biases are corrected, the ratio value for ambiguity resolution increases and the fixing rate also improves from 59.79 to 74.44% at B1I frequency.

Keywords BeiDou navigation satellite system · Timing group delay · Signal-in-space range error · Single-point positioning · Real-time kinematic

Introduction

The BeiDou navigation satellite system (BDS), whose official Phase III service was announced in late 2018, currently consists of a mixed constellation of BDS-2 (Phase II) and BDS-3 (Phase III) including geostationary orbit (GEO), inclined geosynchronous orbit (IGSO), and medium Earth orbit (MEO) satellites (CSNO 2018a). With 15 BDS-2 satellites and 18 BDS-3 satellites in orbit by the end of May 2019, BDS can provide global positioning, navigation, and timing (PNT) service with a positioning accuracy within 10 m (95%) in horizontal and vertical directions (CSNO 2018b). Recent research results with real data show that the global positioning accuracy of BDS is within 2 m (95%) in horizontal and 4 m (95%) in vertical directions (CSNO-TARC 2019; Zhang et al. 2019), which is competitive with GPS. By the end of 2020, with the continuous launching of BDS-3 satellites and the retirement of BDS-2 satellites, a better PNT service for BDS will be available from the standpoints of accuracy, continuity, availability, and integrity.

According to the interface control document (ICD) of BDS, the coordinate system of BDS adopts the BeiDou coordinate system (BDCS) defined by China Geodetic Coordinate System 2000 (CGCS2000), which is aligned with the latest International Terrestrial Reference Frame (ITRF) (CSNO 2018c). As for the time system, BDS adopts the BeiDou navigation satellite system time (BDT), which

✉ Nobuaki Kubo
nkubo@kaiyodai.ac.jp

1 Tokyo University of Marine Science and Technology, Tokyo 1358533, Japan

2 Shanghai Key Laboratory of Space Navigation and Positioning Techniques, Shanghai 200030, China

3 Shanghai Astronomical Observatory, Shanghai 200030, China

4 College of Surveying and Geo-Informatics, Tongji University, Shanghai 200092, China

Published online: 17 December 2019

connects UTC via UTC (NTSC), and is synchronized with UTC within 50 ns. By comparing the broadcast orbits with the precise orbit provided by the Center for Orbit Determination in Europe (CODE), Nicolini et al. (2018) conclude that the BDS IGSO broadcast reference frame is offset by at most 0.31 m in Y direction and the maximum rotation is 3.6 mas in Z direction while for MEO satellites, it is on the same order of magnitude, but with higher uncertainty. With the continuous updates of BDS monitoring station coordinates, the difference between the BDS reference frame and ITRF is expected to become smaller (Zhao et al. 2019).

The signal-in-space range error (SISRE) is a typical quantity indicating the quality of the broadcast ephemeris (Heng et al. 2011). Montenbruck et al. (2015) assess the one-year performance of BDS-2 SISRE and conclude that the SISRE of BDS-2 shows a better consistency of 1.1 m in RMS after multi-GNSS experiment (MGEX) differential code bias (DCB) correction compared to 1.5 m using broadcast timing group delay (TGD) correction, which is attributed to the more accurate MGEX DCB products. Zhang et al. (2016) further suggest that this might be due to the bias of the channel difference between the BDS monitoring station receivers and other commercial receivers. Since July 2017, this bias has notably decreased and the consistency between BDS TGD and MGEX DCB is significantly improved (Wang et al. 2019a, b).

With the implementation of the BDS-3 satellite, BDS achieves better precise orbit determination (POD) results with the contribution of inter-satellite link and higher stability of rubidium clocks and passive hydrogen maser clocks (Tang et al. 2018; Wu et al. 2018; Xie et al. 2019), which improves the SISRE performance. Yang et al. (2019) first give four-day SISRE results of eight BDS-3 satellites, comparing the broadcast ephemeris and POD results from the International GNSS Monitoring and Assessment System (iGMAS), which shows that the average SISRE of BDS-3 is approximately 0.44 m. Zhang et al. (2019) use 2 months of data and compare the SISRE performance of the current BDS constellation with the precise products provided by Wuhan University. They conclude that the SISRE of BDS-3 is smaller than that of BDS-2 satellites, showing an accuracy of 0.71 m versus 0.97 m. However, all these results separate BDS-3 from BDS-2 when assessing the SISRE, as BDS-2 and BDS-3 are the 2nd and 3rd phases of BDS constellation, and users can arbitrarily select the regional BDS-2 or global BDS-3.

Unlike other GNSSs, the code observations of BDS seem to exhibit a complex bias characteristic. Wanninger and Beer (2015) first report the elevation-dependent and frequency-dependent code biases with a variation of more than 1 m for the BDS IGSO and GEO satellites. Lou et al. (2017) further investigate the code biases of the BDS GEO satellites. The corresponding code biases correction models are satellite dependent and can be applied to all types of receivers. It is found that these elevation-dependent code biases are significantly reduced for BDS-3 satellites, especially for B2a, B2b, and B3I signals (Zhang et al. 2017; Yang et al. 2018). Except for satellite elevation-dependent code biases, Gong et al. (2018) find that there still exists a receiver-type-dependent code bias for BDS-2. A set of correction values for different types of receivers are given based on the ionospheric-free combination.

We assess the overall SISRE performance combining BDS-2 and BDS-3 with 5 months of data from day of year (DOY) 6 to 145 in 2019. An apparent pair of clock and TGD biases are found between BDS-2 and BDS-3. To further validate the existence of the biases, long-term globally distributed MGEX stations with different types of receivers are used, and the biases are calibrated. The calibrated clock and TGD biases are then applied and compared using single-point positioning (SPP) and real-time kinematic (RTK) positioning. Finally, some discussions about the biases are presented, followed by the conclusions.

SISRE of BDS

The combined orbit and clock SISRE of the BDS broadcast ephemeris can be expressed as (Montenbruck et al. 2015):

$$\mathrm{SISRE} = \begin{cases} \sqrt{(0.99 \cdot R - \mathrm{Clk})^2 + \frac{1}{126}(A + C)^2}, & \text{for GEO, IGSO} \\ \sqrt{(0.98 \cdot R - \mathrm{Clk})^2 + \frac{1}{54}(A + C)^2}, & \text{for MEO} \end{cases} \tag{1}$$

where R, A, and C denote the orbit error in the radial, along-track, and cross-track directions and Clk denotes the clock offset error.

The orbit and clock error of the broadcast ephemeris can be obtained by a comparison with precise post-processed products. From January 1, 2019, Wuhan University began releasing BDS-2 and BDS-3 precise orbit and clock products (WUM) (ftp://igs.ensg.ign.fr/pub/igs/products/mgex/). When comparing the BDS broadcast ephemeris with WUM products, the difference in the time and coordinate reference system, satellite antenna offset correction, and clock offset correction should be considered (Zhang et al. 2019).

It is known that the satellite clock in the BDS broadcast ephemeris is referred to the B3I signal (CNSO, 2018a), while for WUM precise clocks, it is based on a B1I/B3I ionospheric-free combination (Wang et al. 2019a, b). Thus, the frequency bias difference should be corrected by TGD or DCB. The correction can be expressed as follows when aligned to different frequencies (Ge et al. 2017; Montenbruck et al. 2018):

$$\begin{aligned}\mathrm{Corr}_{\mathrm{B1I}} &= \mathrm{TGD}_1 + \frac{f_3^2}{f_1^2 - f_3^2}\mathrm{DCB}_{\mathrm{B1I/B3I}} \\ \mathrm{Corr}_{\mathrm{B3I}} &= \frac{f_1^2}{f_1^2 - f_3^2}\mathrm{DCB}_{\mathrm{B1I/B3I}} \\ \mathrm{Corr}_{\mathrm{B1I/B3I}} &= \frac{f_1^2}{f_1^2 - f_3^2}\mathrm{TGD}_1\end{aligned} \tag{2}$$

where TGD_1 is the TGD correction from B3I to B1I, which can be derived from the broadcast ephemeris. f_1 and f_3 denote the frequencies of the BDS at B1I and B3I, and $\mathrm{DCB}_{\mathrm{B1I/B3I}}$ stands for the DCB correction from B3I to B1I.

In this study, the DCB corrections provided by the Chinese Academy of Science (CAS) are used, which include multi-GNSS DCB corrections of GPS, GLONASS, Galileo, BDS, and QZSS at an accuracy of 0.2–0.6 ns (Wang et al. 2016).

To assess the SISRE performance with the current BDS constellation, we use 5 months of data from DOY 6 to 145 (GPS week 2035 to 2054) in 2019. When assessing the SISRE results, the BDS-2 and BDS-3 satellites are treated as a single system and are evaluated together. The data sampling is set as 15 min, and the threshold of gross outlier rejection for the SISRE is set as 10 m.

From (1), we can know that the radial orbit error and the clock offset error, i.e., $\alpha \cdot R - \mathrm{Clk}$, make the greatest contribution to the SISRE. Unlike the SISRE, $\alpha \cdot R - \mathrm{Clk}$ also indicates the direction of the error. To examine the BDS broadcast ephemeris error in detail, the monthly average $\alpha \cdot R - \mathrm{Clk}$ values at B1I, B3I, and B1I/B3I frequencies are analyzed and plotted in Fig. 1. As can be seen, for most satellites, it is well within 1 m at the B1I and B3I frequencies, which indicates that a SISRE result below 1 m can be expected. For the B1I/B3I combination, it is interesting that an apparent system bias of more than 2 m between the BDS-2 and BDS-3 satellites is observed. If one examines the B3I frequency closely, a small but unobvious bias can also be observed.

To further investigate and confirm these biases, we separate the BDS-2 and BDS-3 satellites into different groups. The weekly $\alpha \cdot R - \mathrm{Clk}$ average and standard deviation (STD) values between BDS-2 and BDS-3, i.e., $\mathrm{Average}(\alpha \cdot R - \mathrm{Clk})_{\mathrm{BDS-3}} - \mathrm{Average}(\alpha \cdot R - \mathrm{Clk})_{\mathrm{BDS-2}}$ are calculated and depicted in Fig. 2. Again, the system biases at each frequency can be clearly observed, especially for B1I/B3I. Furthermore, the time variation of these biases is quite stable with an STD value within 1 m. The overall 5-months average and STD value for each frequency are summarized in Table 1. Overall system biases of 0.38 m, −0.62 m, and 2.30 m are found at the B1I, B3I, and B1I/B3I frequencies, with STD values of 0.58 m, 0.63 m, and 0.86 m, respectively.

According to (1) and (2), this type of bias may arise from the system bias of the clock and the TGD between the broadcast and post-processed products. Let dt be the clock bias between BDS-2 and BDS-3 obtained by comparing the broadcast clock and the WUM precise clock, and $dtgd_1$ be the TGD bias between BDS-2 and BDS-3 obtained by

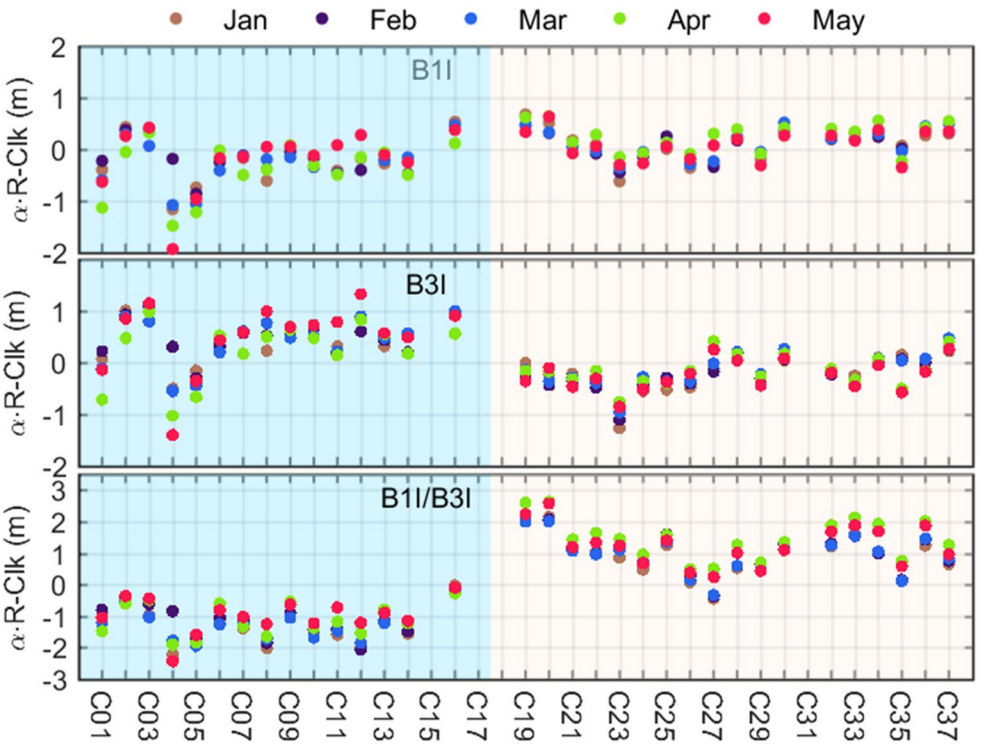

Fig. 1 Monthly average value of BDS $\alpha \cdot R - \mathrm{Clk}$ in 2019 at B1I, B3I, and B1I/B3I frequencies. BDS-2 and BDS-3 are separated by different background colors

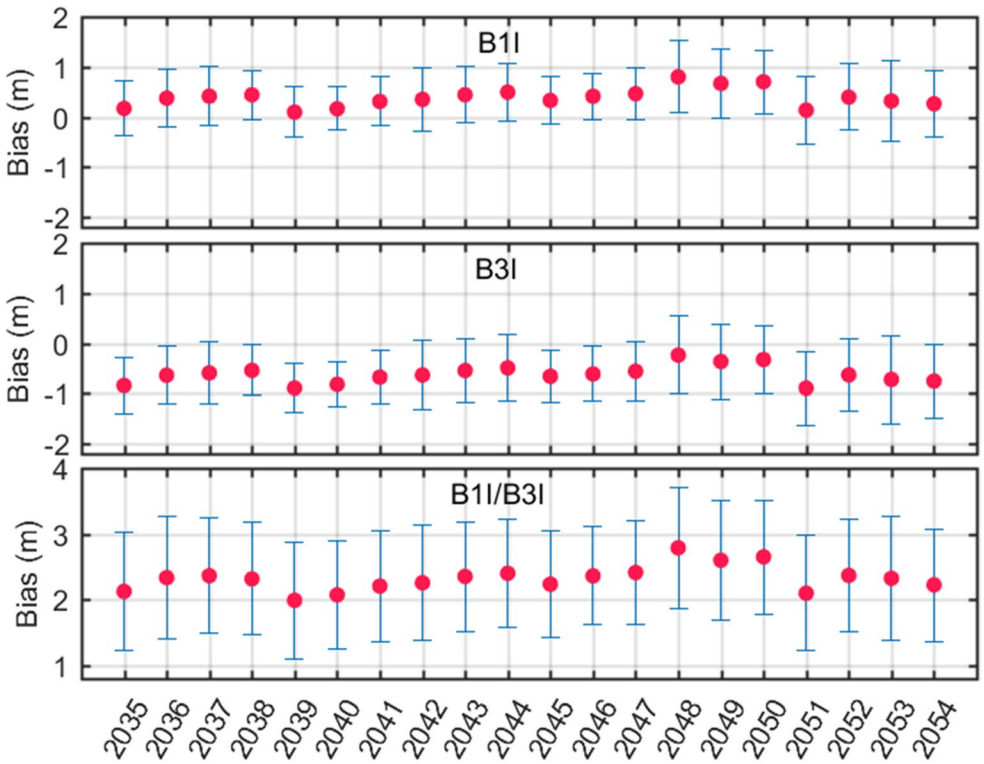

Fig. 2 Average weekly $\alpha \cdot R -$ Clk difference between BDS-2 and BDS-3 at B1I, B3I, and B1I/B3I frequencies. The x-axis unit is GPS week. The error bar stands for the standard deviation of the difference

Table 1 Five-months average $\alpha \cdot R -$ Clk bias between BDS-2 and BDS-3 (in meters)

Frequency	Average	STD
bias_{B1I}	0.38	0.58
bias_{B3I}	−0.62	0.63
$\text{bias}_{\text{B1I/B3I}}$	2.30	0.86

comparing TGD_1 and $\text{DCB}_{\text{B1I/B3I}}$. If the clock and TGD biases do exist between BDS-2 and BDS-3, it follows this relationship:

$$\begin{aligned} dt - dtgd_1 &= \text{bias}_{\text{B1I}} \\ dt &= \text{bias}_{\text{B3I}} \\ dt - \frac{f_1^2}{f_1^2 - f_3^2} dtgd_1 &= \text{bias}_{\text{B1I/B3I}} \end{aligned} \tag{3}$$

where bias_{B1I}, bias_{B3I}, and $\text{bias}_{\text{B1I/B3I}}$ are the $\alpha \cdot R - Clk$ biases at the B1I, B3I, and B1I/B3I frequencies, which are shown in Table 1.

Equation (3) indicates that dt has a positive correlation with the satellite clock, while $dtgd_1$ shows a negative correlation, which agrees with the TGD correction on the satellite clock (CSNO 2018a). By applying the least-squares method, dt and $dtgd_1$ can be easily derived. From the values provided in Table 1, we can deduce that dt is −0.62 m and $dtgd_1$ is −0.99 m.

To further validate the existence of the clock and TGD biases, we apply them in the SISRE assessment. Figure 3 shows the 5-months SISRE results of each BDS satellite at B1I, B3I, and B1I/B3I frequencies with and without the clock and TGD biases correction. From the comparison, we can see that after the bias corrections, the SISRE on most satellites improves at B3I and B1I/B3I while for B1I, the improvement is not apparent. As a statistical result, the average SISRE performance of BDS-2 and BDS-3 is given in Table 2. From the table, we can arrive at the following conclusions:

1. In general, the SISRE performance of BDS-3 is better than that of BDS-2. This is expectable as more stable satellite clocks and inter-satellite link techniques are employed in BDS-3 satellites (Wu et al. 2018; Tang et al. 2018).
2. For the B1I frequency, the overall SISRE is 0.70 m versus 0.72 m after the clock and TGD correction, which means that the biases do not have much of an impact on the B1I frequency. However, for the B3I and B1I/B3I frequencies, the SISRE improves for both BDS-2 and BDS-3, especially for B1I/B3I, in which case the overall SISRE improves from 1.41 to 0.84 m. This is reasonable as the TGD bias would increase by a factor of 2.94, according to (3).
3. When the clock and TGD biases are corrected, the BDS SISRE performance is like the results presented

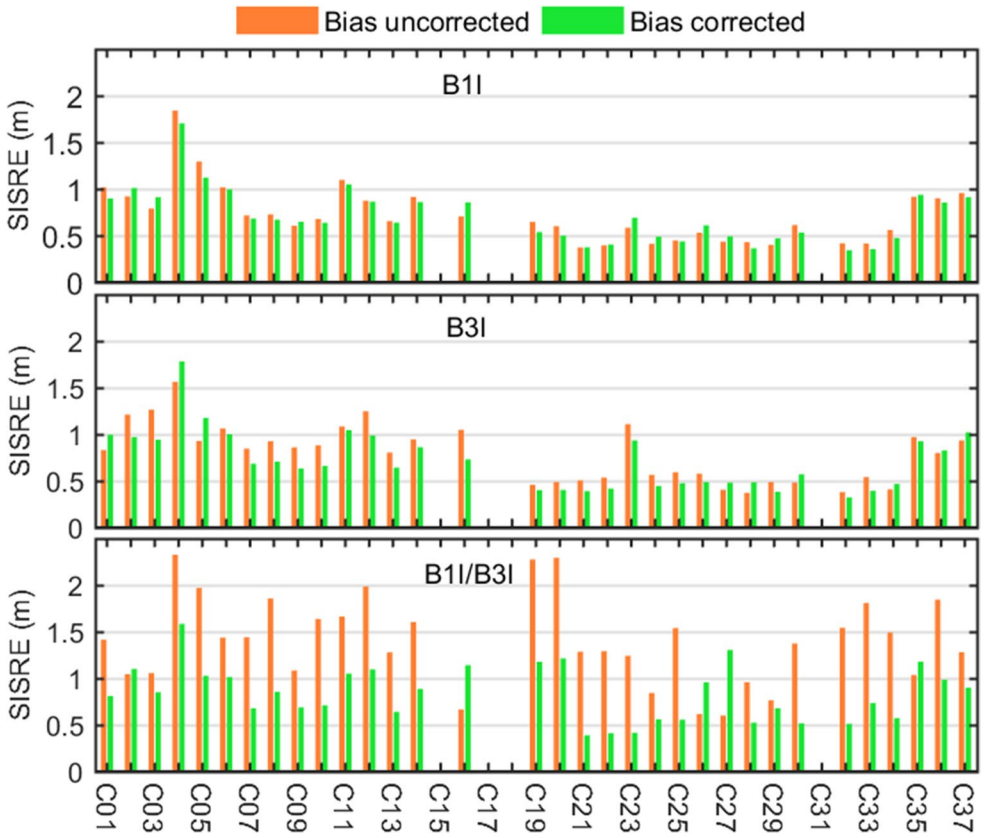

Fig. 3 RMS of BDS SISRE at B1I, B3I, and B1I/B3I frequencies with and without the clock and TGD biases correction for BDS-2 and BDS-3

Table 2 BDS SISRE statistics before and after the clock and TGD biases correction (in meters)

Type	Frequency	BDS-2	BDS-3	BDS
Bias uncorrected	B1I	0.92	0.55	0.72
	B3I	1.03	0.59	0.79
	B1I/B3I	1.50	1.34	1.41
Bias corrected	B1I	0.90	0.54	0.70
	B3I	0.92	0.54	0.72
	B1I/B3I	0.94	0.75	0.84

by Zhang et al. (2019), where the SISRE of BDS-2 and BDS-3 is evaluated separately. This indicates that the biases corrections are constant values and can be removed.

4. After the clock and TGD biases correction, the SISRE of BDS-2 shows a similar performance at each frequency, while that of BDS-3 is much worse at B1I/B3I. This may be attributed to the amplification of the TGD and DCB difference for BDS-3. To verify this, the difference between TGD_1 and $DCB_{B1I/B3I}$ is compared using the value on DOY 60, 2019, which is listed in Table 3. It is shown that the STD of the TGD_1 and $DCB_{B1I/B3I}$ difference for BDS-3 is larger than that for BDS-2, which indicates the poor capability of the BDS control segment in tracking BDS-3 satellites (Wang et al. 2019a, b). Therefore, it would lead to worse SISRE performance at B1I/B3I than at B1I for BDS-3, according to (2). Meanwhile, it is found that the average value of the TGD_1 and $DCB_{B1I/B3I}$ difference for BDS-2 and BDS-3 is 1.04 m, which agrees with the estimated TGD bias of −0.99 m from (3).

Table 3 TGD_1 and $DCB_{B1I/B3I}$ difference for BDS-2 and BDS-3 (in meters)

Type	BDS-2	BDS-3
Average	−0.27	0.77
STD	0.17	0.29

BDS clock and TGD biases estimation

The above-estimated clock and TGD biases use the WUM and the CAS DCB products as the reference value. In other words, it is just the difference from the reference value. To derive the absolute biases of the broadcast clock and the TGD, we propose a method based on BDS raw measurements in this section.

Estimation method

For the BDS raw measurements of the pseudorange, the observation equations at B1I and B3I can be expressed as follows:

$$\begin{aligned} P_1 &= \rho + t_{\mathrm{rcv}_1} - t^{\mathrm{sat}} + \delta_{\mathrm{trop}} - \frac{\delta_{\mathrm{iono}}}{f_1^2} + \delta_{tgd_1} + \delta_{P_1} \\ P_3 &= \rho + t_{\mathrm{rcv}_3} - t^{\mathrm{sat}} + \delta_{\mathrm{trop}} - \frac{\delta_{\mathrm{iono}}}{f_3^2} + \delta_{P_3} \end{aligned} \tag{4}$$

where P_i is the raw measurement of the pseudorange at frequency i, t_{rcv_i} is the receiver clock including the receiver hardware delay at frequency i, t^{sat} is the satellite clock referring to B3I, δ_{trop} and δ_{iono} are the tropospheric and ionospheric delays, δ_{tgd_1} is the TGD correction from B3I to B1I, and δ_{P_i} is the pseudorange observation noise.

To eliminate the first-order ionospheric delay, we apply the dual-frequency ionospheric-free (IF) combination:

$$P_{\mathrm{IF}} = \rho + t_{\mathrm{rcv}_{\mathrm{IF}}} - t^{\mathrm{sat}} + \delta_{\mathrm{trop}} + \frac{f_1^2}{f_1^2 - f_3^2}\delta_{tgd_1} + \delta_{P_{\mathrm{IF}}} \tag{5}$$

Assuming that the clock and TGD biases exist between BDS-2 and BDS-3, for BDS-3 satellites, the single- and dual-frequency observations are then changed to the following:

$$\begin{cases} P_1 = \rho + t_{\mathrm{rcv}_1} - \left(t^{\mathrm{sat}} + \mathrm{bias}_{\mathrm{B1I}}\right) + \delta_{\mathrm{trop}} - \frac{\delta_{\mathrm{iono}}}{f_1^2} + \delta_{tgd_1} + \delta_{P_1} \\ P_3 = \rho + t_{\mathrm{rcv}_3} - \left(t^{\mathrm{sat}} + \mathrm{bias}_{\mathrm{B3I}}\right) + \delta_{\mathrm{trop}} - \frac{\delta_{\mathrm{iono}}}{f_3^2} + \delta_{P_3} \\ P_{\mathrm{IF}} = \rho + t_{\mathrm{rcv}_{\mathrm{IF}}} - \left(t^{\mathrm{sat}} + \mathrm{bias}_{\mathrm{B1I/B3I}}\right) + \delta_{\mathrm{trop}} + \frac{f_1^2}{f_1^2 - f_3^2}\delta_{tgd_1} + \delta_{P_{\mathrm{IF}}} \end{cases} \tag{6}$$

For a static station with a known position, the station coordinates can be fixed precisely. The satellite coordinates, satellite clock, and TGD can be derived from the broadcast ephemeris. The tropospheric and ionospheric delays can be corrected by model. Hence, the estimated parameters are the receiver clocks and the biases correction at each frequency. If both BDS-2 and BDS-3 satellites are tracked at one station, the biases at each frequency can be estimated. The clock and TGD biases can then be derived using (3).

The stochastic model of the pseudorange observation is as follows:

$$\sigma^2 = \sigma_{\mathrm{SISRE}}^2 + \sigma_{\mathrm{Trop}}^2 + \sigma_{\mathrm{Iono}}^2 + \sigma_{\mathrm{Meas}}^2 \tag{7}$$

where σ is the variance of the code observation, while σ_{SISRE}, σ_{Trop}, σ_{Iono}, and σ_{Meas} stand for the SISRE of the BDS satellites, tropospheric error after model correction, ionospheric error after model correction, and the measurement noise of the pseudorange.

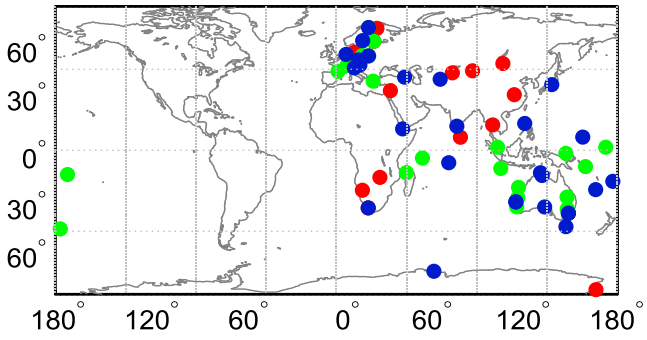

Fig. 4 Sixty-eight selected MGEX stations. The red, green, and blue circles stand for stations equipped with Javad, Trimble, and Septentrio receivers, respectively

Table 4 Receiver information

Receiver	Types or version	Number	Note
Javad	TRE_3 TRE_3 delta	18	Track all BDS satellites
Trimble	Alloy NETR9 5.3.7	23	Cannot track C31–C37
Septentrio	POLARX5TR POLARX5	27	Cannot track B3I signal of C16, C23–C27, C29–C30, C35–C37

Data collection

For the estimation of the clock and TGD biases, 68 globally distributed MGEX stations are selected, as shown in Fig. 4. To track more BDS-2 satellites, we excluded the stations located around the Americas. Among the selected stations, all of them are able to track the B1I and B3I data of BDS-2 and BDS-3. The receiver information of these stations is summarized in Table 4. For statistical and long-term results, observation data of every first day of the week from GPS week 2041 to 2054 are collected at these stations.

Estimated results

During the estimation of the clock and TGD biases, the data interval is set as 30 s. The cutoff elevation is set as 10°, and observations with a position dilution of precision (PDOP) value higher than 6 are rejected. The tropospheric delay is corrected by the GPT2w and the VMF model (Böhm et al. 2015). The ionospheric delay is corrected by the ionospheric grid model provided by the International GNSS Service (IGS) (ftp://cddis.gsfc.nasa.gov/pub/gps/products/ionex/). The station coordinates are fixed by IGS daily solutions. The receiver clock is estimated as a parameter with white noise, while the bias is estimated as a constant parameter. For a more precise estimation of the bias, the pseudorange is smoothed by the carrier phase.

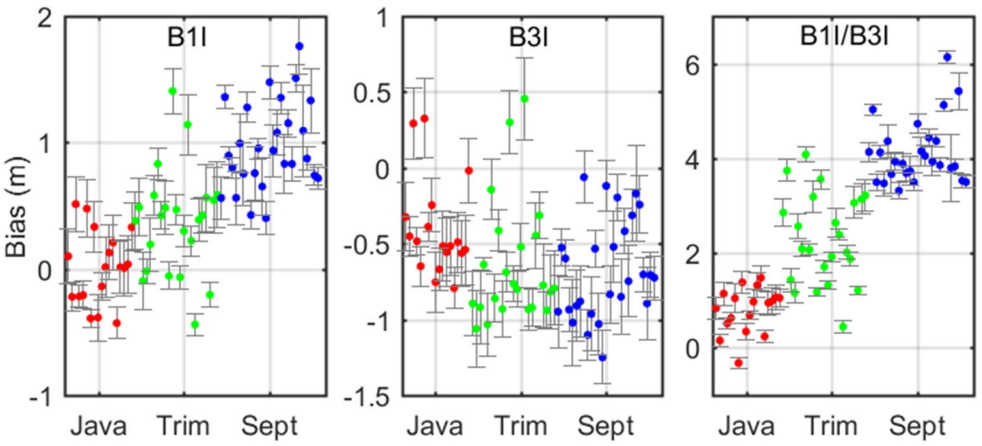

Fig. 5 Estimated bias at B1I, B3I, and B1I/B3I frequencies. The error bar stands for the standard deviation at each station. The red, green, and blue circles stand for stations equipped with Javad, Trimble, and Septentrio receivers

Table 5 Estimated bias between BDS-2 and BDS-3 at different frequencies (in meters)

Frequency	Javad		Trimble		Septentrio	
	Average	STD	Average	STD	Average	STD
B1I	0.01	0.33	0.37	0.45	0.96	0.38
B3I	−0.41	0.36	−0.65	0.44	−0.67	0.37
B1I/B3I	0.81	0.51	2.30	0.95	4.12	0.61

Using 14 days of data out of 14 weeks, we estimate the bias at each station. Figure 5 depicts the average and the STD value of the estimated biases for the B1I, B3I, and B1I/B3I frequencies. It can be observed that a bias does exist at each station, especially for the B1I/B3I frequency. Furthermore, the biases disperse depending on the receiver type, which is evident on the Javad and Septentrio receivers. The statistical results for different receiver types are given in Table 5 for an overall observation of the biases. We can see that the bias for B3I, which is between −0.41 and −0.67 m, seems similar among the three receivers. However, for the B1I frequency, the average bias is 0.01 m and 0.97 m for Javad and Septentrio receivers, while it reaches 0.81 m and 4.12 m on B1I/B3I frequency. Further, the STD value of the bias for B1I/B3I is larger than that for the other single frequencies, which may be due to the amplification of the observation noise after ionospheric-free combination. It appears that the STD value of the bias for the Trimble receiver is larger than the corresponding values for the Javad and Septentrio receivers, which can also be observed in Fig. 5.

According to (3), the clock and TGD biases for each type of receiver can be estimated. As the clock bias also affects carrier phase observations, it is better to estimate it as a common value for all types of receivers. Therefore, the estimated clock and TGD biases are listed in Table 6. Whereas the value is −0.62 m using the SISRE assessment in the previous section, the estimated clock bias is −0.58 m using raw observations. Although the TGD bias is different at each receiver, reaching a value of −0.48, −0.98, and −1.60 m for Javad, Trimble, and Septentrio receiver, we can also see that the average value is approximately −1.02 m, which also agrees with the value of −0.99 m from the SISRE assessment.

Table 6 Calibrated clock and TGD biases between BDS-2 and BDS-3 for different receivers (in meters)

	Javad	Trimble	Septentrio
dt	−0.58	−0.58	−0.58
$dtgd_1$	−0.48	−0.98	−1.60

Impact of the clock and TGD biases on positioning

As discussed above, the existence of clock and TGD biases between BDS-2 and BDS-3 has been proved. In this section, the impact of the clock and TGD biases on the positioning will be assessed from the standpoints of SPP and RTK.

SPP

For a comprehensive assessment of the comparison in SPP, four schemes of handling the clock and TGD biases are executed:

1. Scheme 1 (S1): Normal SPP with one receiver clock.
2. Scheme 2 (S2): Estimate the intra-system bias between BDS-2 and BDS-3.

3. Scheme 3 (S3): Correct the clock and TGD biases using values of − 0.62 and − 0.99 m, respectively.
4. Scheme 4 (S4): Correct the clock and TGD biases using values calibrated according to the receiver type.

For the independent validation of clock and TGD bias, 1 week of data from DOY 134 to 140 in 2019 is collected at the 68 MGEX stations. For the processing of SPP, satellite orbit, clock, and TGD corrections are derived from the broadcast ephemeris. The cutoff elevation is set as 10°, and observations with a PDOP value higher than 6 are rejected. The tropospheric delay is corrected by GPT2w and the VMF model (Böhm et al. 2015). The ionospheric delay is corrected by the BDS Klobuchar model for single-frequency data and by ionospheric-free combination for dual-frequency data. For Scheme 2, the intra-system bias is estimated as a constant parameter. The other parameters to be estimated in the four schemes are the station coordinates and the receiver clock. The station coordinates from IGS daily final solutions are used as the reference.

Figure 6 illustrates the comparison of the three-dimensional (3D) positioning RMS at the B1I, B3I, and B1I/B3I frequencies using the 1-week data at each station. For a better understanding of the comparison, the results are divided by receiver type, with each receiver type being represented by a different figure background color. The statistical results and improvement of Schemes 2–4 in comparison with Scheme 1 are summarized in Table 7. The following can be concluded:

1. For all the three types of receivers, the improvement for Scheme 4 is slightly better than that for Scheme 3. This indicates that the precision of the calibrated clock and TGD biases is better than that of the biases from the SISRE assessment.
2. Among the three types of receivers, the improvement for the Septentrio and Trimble receivers is more apparent than that for the Javad receiver. This may because the clock and TGD corrections for the Javad receiver are within 1 m, and therefore, it does not contribute much to SPP considering the BDS SISRE, ionospheric model error, and observation noise.
3. Among the three frequencies, B1I/B3I improves the most in Scheme 2 and Scheme 4, especially for the Septentrio receiver, which shows an improvement of 31.8%. For the Trimble receiver, an improvement in the range 19.7–21.6% is seen. From Table 6, it is seen that the $dtgd_1$ bias on the Septentrio and Trimble receivers can be as large as − 0.98 m and − 1.60 m, which will increase by a factor of 2.94 after the ionospheric-free combination of B1I/B3I.

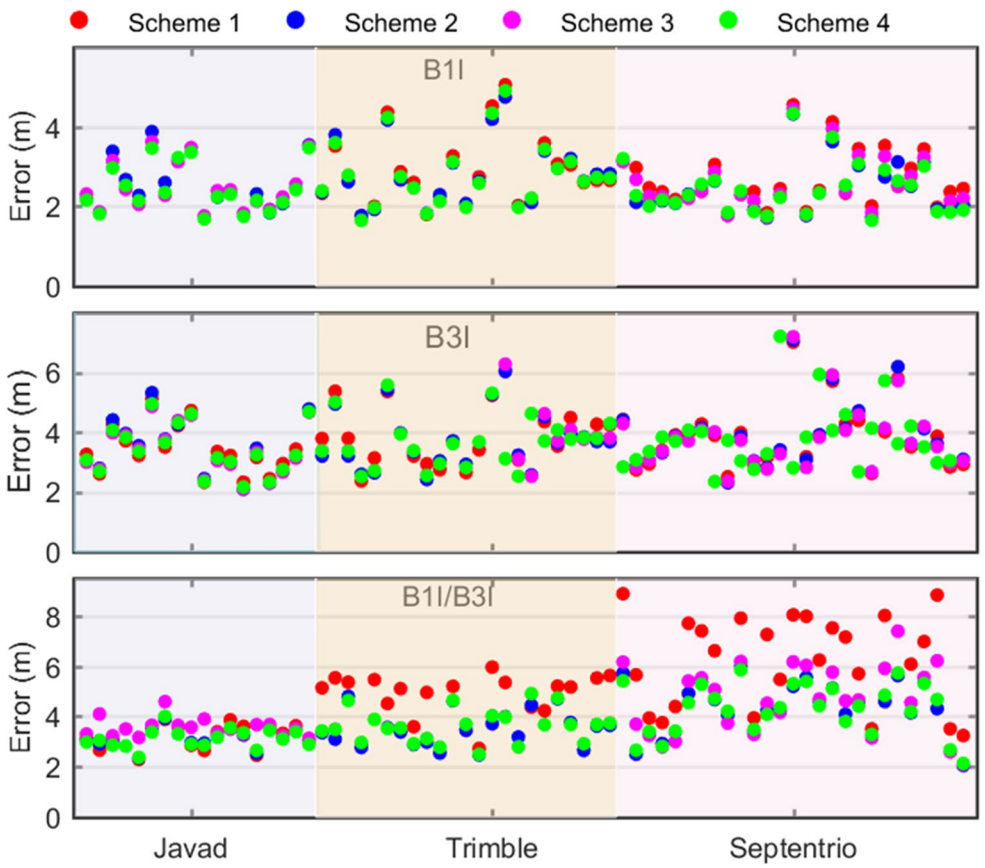

Fig. 6 SPP performance of the four schemes for different types of receivers at B1I, B3I, and B1I/B3I frequencies. The y-axis represents the 1-week 3D RMS of the positioning error at each station. The *x*-axis represents the stations, which are divided by the receiver types Javad, Trimble, and Septentrio

Table 7 RMS (m) and improvement (percent) in BDS SPP performance for different schemes. Note that $\text{improv}_{j-i} = (\text{RMS}_{Si} - \text{RMS}_{Sj})/\text{RMS}_{Si}$

Receiver	Freq.	S1 (m)	S2 (m)	S3 (m)	S4 (m)	Improv_{2-1}	Improv_{3-1}	Improv_{4-1}
Javad	B1I	2.43	2.52	2.49	2.42	−3.6	−2.3	0.3
	B3I	3.30	3.29	3.21	3.21	0.3	2.5	2.6
	B1I/B3I	3.17	3.12	3.52	3.10	1.5	−11.2	2.1
Trimble	B1I	2.74	2.72	2.72	2.72	0.6	0.6	0.6
	B3I	3.52	3.37	3.43	3.43	4.2	2.5	2.6
	B1I/B3I	4.44	3.48	3.57	3.56	21.6	19.6	19.7
Septentrio	B1I	2.63	2.43	2.52	2.43	7.7	4.3	7.7
	B3I	3.50	3.42	3.44	3.44	2.3	1.6	1.6
	B1I/B3I	6.25	4.26	4.65	4.26	31.8	25.5	31.8

4. When comparing Scheme 2 with Scheme 4, it is seen that the Septentrio receiver shows similar performance in both schemes. For the Javad receiver, Scheme 4 is slightly better than Scheme 2. However, for the Trimble receiver, the conclusion is unlike that for the Javad receiver. This can be interpreted as a trade-off estimation strategy. On the one hand, when the intra-system bias is estimated, the strength of the SPP model would become weaker. On the other hand, the clock and TGD biases seem to be more dispersive for the Trimble receiver, as shown in Fig. 5 and Table 5. Therefore, when the clock and TGD biases and the STD are small, it is better to use the calibrated model for correction. When the clock and TGD biases are more dispersive such as in the case of the Trimble receiver, it is better to perform the estimation by adding an intra-system bias. However, we should note that in this case at least five satellites are required.

For a spatial observation of the impact of the clock and TGD biases in SPP, the station-dependent SPP results comparing Scheme 1 and Scheme 4 at the B1I/B3I frequency are shown in Fig. 7. The improvement outside the Asia–Pacific region is much more obvious. This may be attributed to the decreased number of BDS-2 satellites outside the Asia–Pacific region (Zhang et al. 2019). Therefore, when fewer BDS-2 satellites are visible, the contribution of the clock and TGD biases would be more significant for BDS-2 and BDS-3 combined SPP.

Furthermore, for a more specific observation of the contribution of the clock and TGD biases, we take one of the stations, STR1 (35.32°S, 149.01°E), as an example. Figure 8 depicts the visible satellite period on May 15, 2019. Note that the B3I signal of some BDS-3 satellites cannot be tracked, as STR1 is equipped with the Septentrio receiver.

The SPP results for horizontal and vertical components comparing Scheme 1 and Scheme 4 at the B1I and B1I/B3I frequencies are examined, as shown in Fig. 9. The positioning error decreases from 3.49 m to 2.27 m in the horizontal and from 6.26 to 4.33 m in the vertical for the

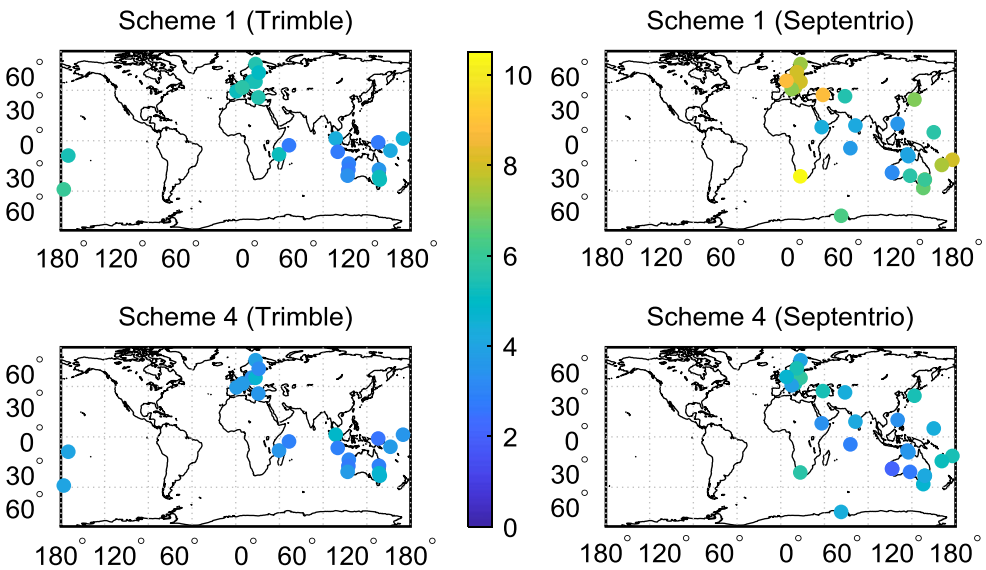

Fig. 7 RMS of 3D positioning error of B1I/B3I SPP for Trimble (left) and Septentrio (right) receiver

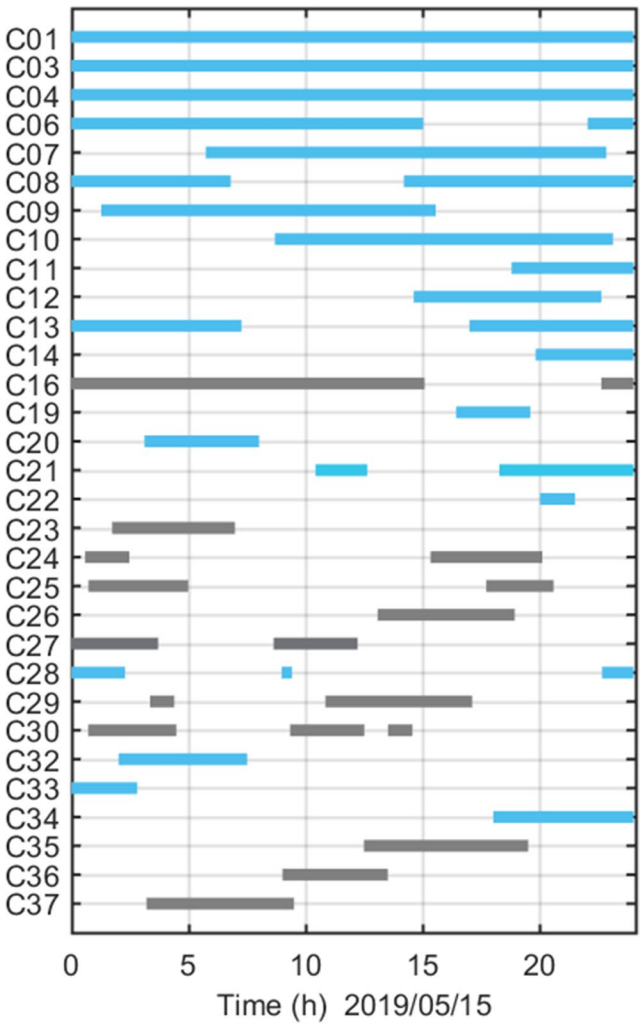

Fig. 8 Visible satellite period at STR1 on May 15, 2019. The gray bar indicates that only B1I data are available, and the light blue bar indicates that both B1I and B3I data are available

B1I/B3I frequency. A similar improvement can also be found for the B1I frequency. Furthermore, the positioning error would be more centered at the zero-mean value.

According to Guo et al. (2015) and Chen et al. (2015), the unmodeled bias will be absorbed by the other parameters and positioning residuals. The clock and TGD biases would also affect the clock parameter and post-fit observation residuals in SPP. Figure 10 depicts the corresponding positioning residuals of SPP at STR1. From the figure, we can see that when the clock and TGD biases are corrected, the overall RMS of the residuals decreases from 1.67 m and 0.81 m to 1.00 m and 0.65 m for B1I/B3I and B1I, respectively. Although it is not shown in this contribution, it is expected that the accuracy of the estimated receiver clock would also improve after the clock and TGD biases correction.

RTK

The above research shows that the TGD biases are receiver-type-dependent. Therefore, a bias difference for different types of receivers would still exist after double differencing. Consequently, it is expected that the difference in the TGD biases would affect the RTK solutions.

To validate this, a 70-m baseline from STR1 to STR2 on May 15, 2019, is selected. STR1 and STR2 are equipped with the Septentrio and Trimble receivers, respectively. For the RTK strategy, the single-epoch ambiguity resolution (AR) method without considering the troposphere and ionosphere difference is applied. A threshold of 3.0 is set for the ratio test using the LAMBDA method (Teunissen 1995). To reduce the impact of noise from low-elevation satellites, we set the cutoff elevation angle as 10° for the float solution in the Kalman filter and 20° in the procedure for ambiguity fixing. The AR fixing rate is defined as a ratio value higher than 3.0 and a 3D positioning error less than 5 cm compared with the true coordinates in the case of wrong fixing.

For single-epoch AR, the data quality of the pseudorange is quite important. Therefore, the pre-fit double-difference observation minus corrections (OMC) of B1I and B3I are plotted using true coordinates, as shown in Fig. 11. We can see that the variation in OMC at B1I is smaller after the clock and TGD biases correction in Scheme 4. The overall RMS of OMC also decreases from 1.21 to 1.02 m. For the B3I frequency, the OMC remains the same, as the clock correction is eliminated after the double difference. Meanwhile, the observation noise at B3I is much smaller than that at B1I, which has also been proved by other researchers (Zhang et al. 2017; Yang et al. 2018).

The ratio value is a crucial factor indicating the level of confidence in the RTK result. The higher the ratio, the more reliable the AR result. Figure 12 shows the ratio difference with and without the clock and TGD biases correction for baseline STR1–STR2 for the dual frequency (B1I/B3I) and the single frequency (B1I). We can see that for most of the epochs, a higher ratio value can be derived if the clock and TGD biases are corrected. The corresponding fixing rates are shown in Table 8. For dual-frequency data, the fixing rate is the same. For single-frequency RTK at B1I, the fixing rate improves from 59.79 to 74.44%. This is due to the weaker model strength of single-frequency single-epoch RTK, for which case the RTK performance is more sensitive to observation bias or noise.

Discussion

As TGD correction affects the code observations, the TGD bias analyzed in this contribution is similar to the code biases. In our research, we find the existence of a

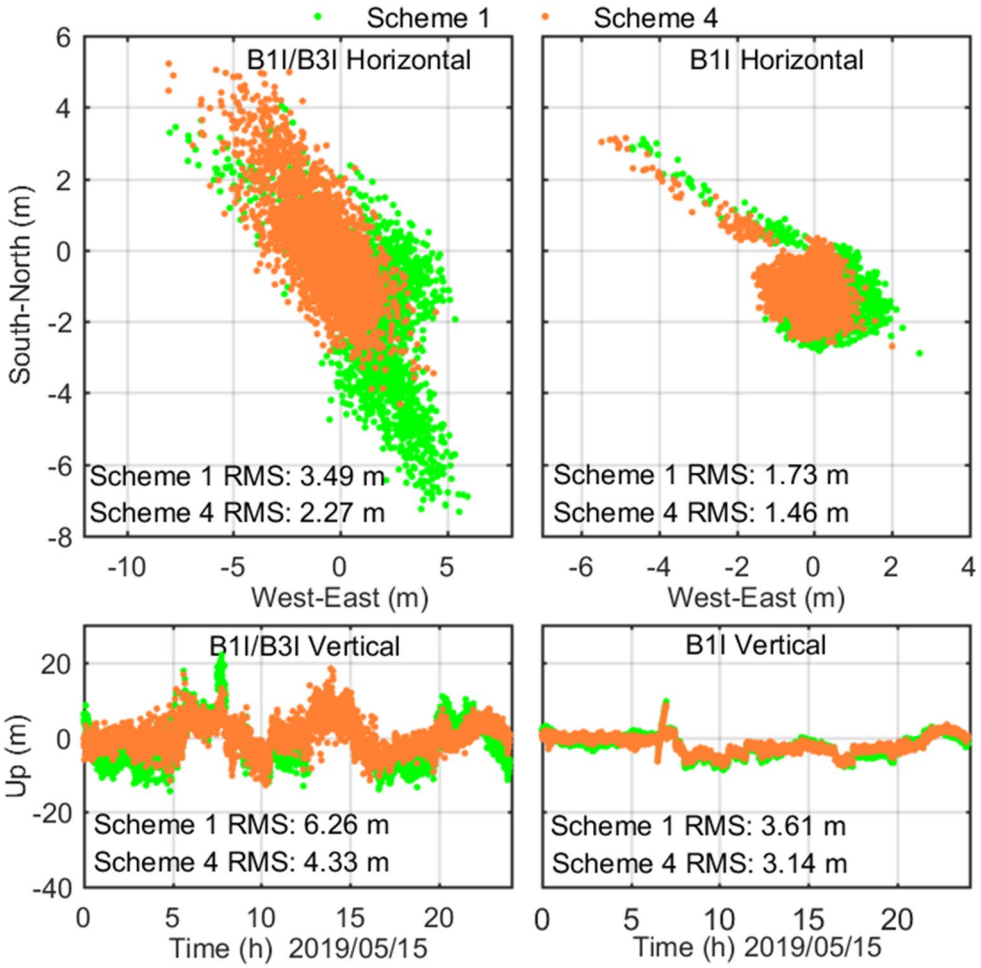

Fig. 9 Horizontal and vertical positioning error of B1I/B3I (left) and B1I (right) SPP at station STR1

receiver-type-dependent TGD bias between BDS-2 and BDS-3. We conclude that this bias will affect different frequencies or frequency combinations at a different level. However, does the bias differ not only between BDS-2 and BDS-3 but also among BDS-3 satellites? Meanwhile, due to the receiver problem, Trimble and Septentrio receivers cannot track all BDS-3 satellites or the B3I signal of all satellites. The missing data may also affect the precision of the estimated bias. With more receivers tracking all BDS-3 satellites in the future, this bias can be further precisely calibrated.

It is also interesting to find that there also exists a clock bias between BDS-2 and BDS-3. Similarly, we can attribute this bias as a TGD bias at the B3I frequency. However, as the bias is so close for each type of receiver in Table 5, it is quite strange that there seems to exist a common offset among BDS monitoring receivers and MGEX receivers between BDS-2 and BDS-3. On other hand, different from other systems, the satellite clock of the BDS broadcast ephemeris is determined by two-way satellite time and frequency transfer (TWSTFT) (Zhou et al. 2016; Pan et al. 2018), which is directly based on B3I frequency and no DCB correction need to be considered. Therefore, in this study, we prefer to assume that this bias may come from the time system bias or clock bias between BDS-2 and BDS-3. However, this needs further investigation as each of these biases—the TGD bias at B3I and the clock bias—will have the same impact on user positioning.

Although the TGD bias or code bias should be aligned to the same basis for different receivers, currently the receiver-type-dependent TGD bias or code bias do exist. Wang et al. (2019a, b) suspect that independent receivers are adopted in BDS-2 and BDS-3 TGD determination. As pointed out by Hauschild and Montenbruck (2016), different multipath mitigation techniques or correlator spacing employed in different receivers may lead to inconsistent code bias. Montenbruck et al. (2014) and Wang et al. (2016) also prove that the selection of different receiver types will affect the estimated satellite TGD/DCB. Therefore, we believe that the TGD bias will still exist as long as different receivers are employed in BDS-2 and BDS-3 control segment.

In this study, we estimate the clock and TGD biases between BDS-2 and BDS-3 on the basis of the broadcast ephemeris. However, due to the precision of the broadcast

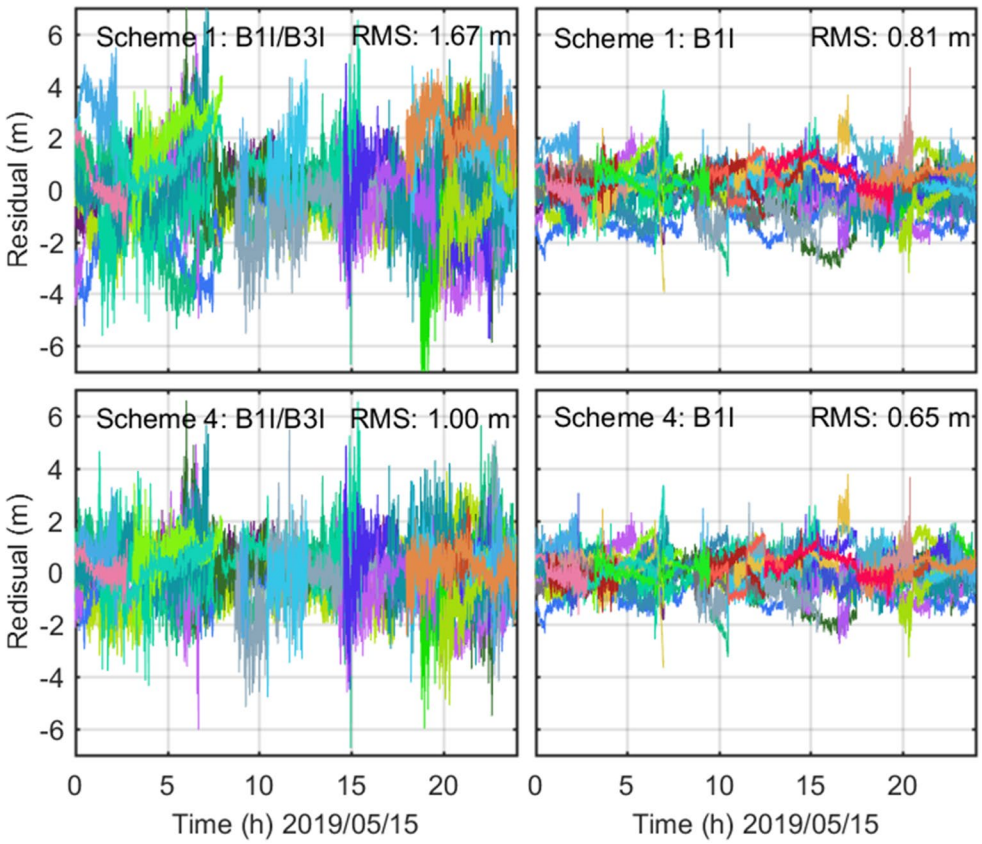

Fig. 10 SPP residuals of B1I/B3I (left) and B1I (right) SPP at station STR1. Different colors indicate different satellites

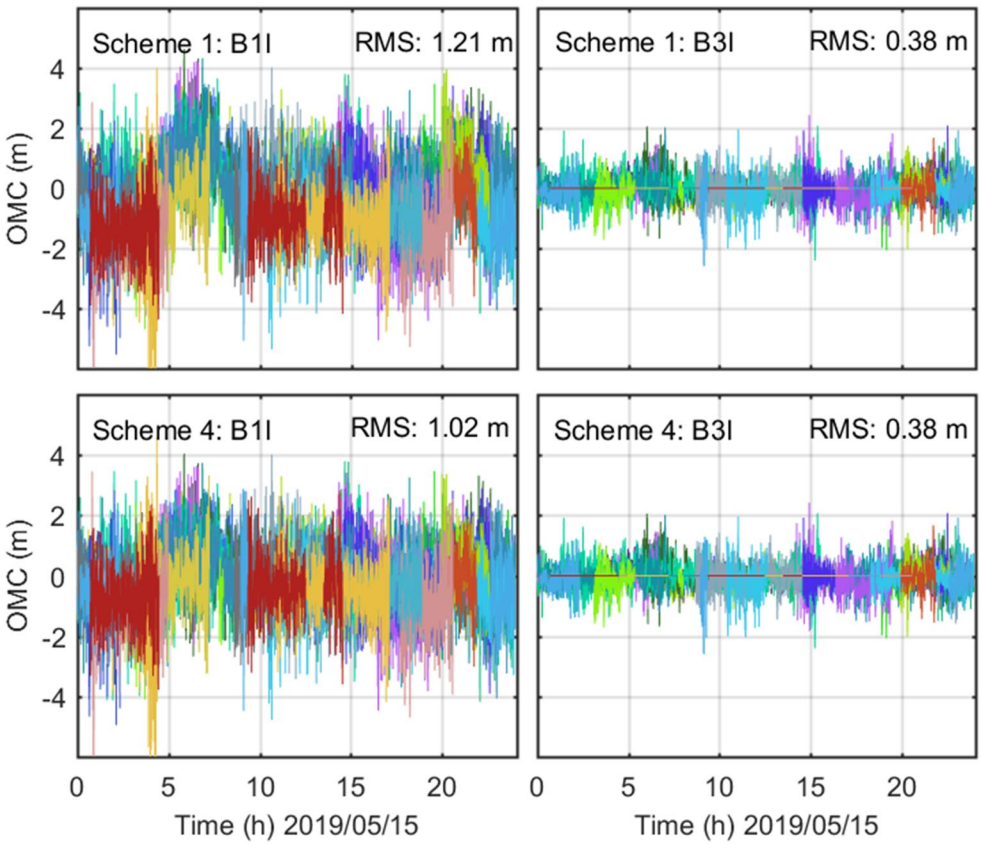

Fig. 11 OMC of B1I (left) and B3I (right) at baseline STR1–STR2. Different colors indicate different satellites

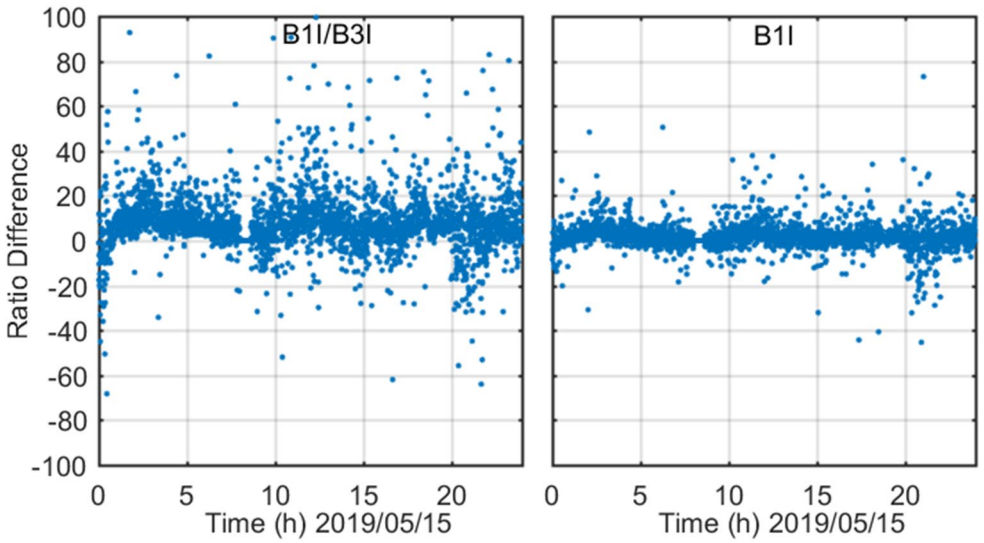

Fig. 12 Ratio difference at baseline STR1–STR2 for B1I/B3I and B1I RTK ambiguity resolution using LAMBDA. A positive value means that the ratio value is higher when the clock and TGD biases are corrected, while a negative value means that the ratio value is lower when the clock and TGD biases are corrected

Table 8 AR fixing rates at baseline STR1–STR2 (ratio > 3 and 3D error < 5 cm)

	Scheme 1 (%)	Scheme 4 (%)
B1I/B3I	99.97	99.97
B1I	59.79	74.44

ephemeris and ionospheric correction, the accuracy of the estimated biases needs to improve further. More accurate orbits and clocks can be used in the future.

For the assessment of the BDS SISRE, if more precise IGS orbit and clock products become available in the future, it is expected that the BDS SISRE would be further improved.

Conclusions

In this contribution, we find the existence of clock and TGD biases between BDS-2 and BDS-3 for BDS broadcast ephemeris. By comparing the WUM final orbit and clock, we deduce that the average clock bias is −0.62 m, while the TGD difference from B3I to B1I is −0.99 m. When the biases are corrected, the 5-months SISRE performance of BDS improves from 1.41 to 0.84 m for the B1I/B3I frequency.

We select 68 MGEX stations equipped with different receivers using 14 days of raw observations spanning 14 weeks to derive the absolute value of clock and TGD biases between BDS-2 and BDS-3. It is found that the clock bias is similar for all receivers, while the TGD bias is receiver type dependent. For the Septentrio receiver, the TGD bias could become as large as −1.6 m and thus would increase to an average bias of 4.12 m for the B1I/B3I frequency, which cannot be ignored. Meanwhile, the average clock and TGD biases of all receivers agree with that from the comparison between the post-processed products and broadcast ephemeris.

Some experiments are carried out to validate the calibrated biases. The SPP results based on the 68 MGEX stations on different days prove that after the clock and TGD biases correction, the positioning RMS improves at a different level for different types of receivers. For spatially related results, the improvement is more evident outside the Asia–Pacific region, where fewer BDS-2 satellites are tracked. For receiver-type-dependent results, the best improvement is 31.8% at the B1I/B3I frequency for the Septentrio receiver. A similar improvement is also observed if the intra-system bias between BDS-2 and BDS-3 is estimated. However, our calibrated value is recommended, as only four satellites are required. For RTK users, when the clock and TGD biases are corrected, the ratio value in ambiguity resolution improves for most of the cases, and the fixing rate for single-frequency B1I RTK also improves.

However, for more accurate calibration of the clock and TGD biases between BDS-2 and BDS-3 or even among the individual satellites, further investigation and a more detailed analysis should be carried out.

Acknowledgements This work is mainly funded by the National Natural Science Foundation of China (No. 41874042 and No. 11673050) and partly sponsored by Opening Project of Shanghai Key Laboratory of Space Navigation and Positioning Techniques (No. KFKT_201705). The GNSS observation data and products provided by IGS are acknowledged. We also thank the Chinese Academy of Science for providing the MGEX DCB values for comparison.

References

Böhm J, Möller G, Schindelegger M, Pain G, Weber R (2015) Development of an improved empirical model for slant delays in the troposphere (GPT2w). GPS Solut 19(3):433–441

Chen J, Zhang Y, Wang J, Yang S, Dong D, Wang J, Qu W, Wu B (2015) A simplified and unified model of multi-GNSS precise point positioning. Adv Space Res 55(1):125–134

CSNO (2018a) BeiDou Navigation satellite system signal in space interface control document open service signal B3I (Version 1.0). China Satellite Navigation Office

CSNO (2018b) Development of the BeiDou navigation satellite system (Version 3.0). China Satellite Navigation Office

CSNO (2018c) BeiDou navigation satellite system open service performance standard (Version 2.0). China Satellite Navigation Office

CSNO-TARC (2019) China-Arab joint BDS test & evaluation results. Test and Assessment Research Center of China Satellite Navigation Office

Ge Y, Zhou F, Sun B, Wang S, Shi B (2017) The impact of satellite time group delay and inter-frequency differential code bias corrections on multi-GNSS combined positioning. Sensors 17(3):602

Gong X, Lou Y, Zheng F, Gu S, Shi C, Liu J, Jing G (2018) Evaluation and calibration of BeiDou receiver-related pseudorange biases. GPS Solut 22(4):98

Guo F, Zhang X, Wang J (2015) Timing group delay and differential code bias corrections for BeiDou positioning. J Geodesy 89(5):427–445

Hauschild A, Montenbruck O (2016) A study on the dependency of GNSS pseudorange biases on correlator spacing. GPS Solut 20(2):159–171

Heng L, Gao G, Walter T, Enge P (2011) Statistical characterization of GPS signal-in-space errors. In: Proceedings of ION ITM 2011. Institute of Navigation, San Diego, San Diego, CA, USA, January 24–26, pp 312–319

Lou Y, Gong X, Gu S, Zheng F, Feng Y (2017) Assessment of code bias variations of BDS triple-frequency signals and their impacts on ambiguity resolution for long baselines. GPS Solut 21(1):177–186

Montenbruck O, Hauschild A, Steigenberger P (2014) Differential code bias estimation using multi-GNSS observations and global ionosphere maps. Navig J Inst Navig 61(3):191–201

Montenbruck O, Steigenberger P, Hauschild A (2015) Broadcast versus precise ephemerides: a multi-GNSS perspective. GPS Solut 19(2):321–333

Montenbruck O, Steigenberger P, Hauschild A (2018) Multi-GNSS signal-in-space range error assessment–methodology and results. Adv Space Res 61(12):3020–3038

Nicolini L, Caporali A (2018) Investigation on reference frames and time systems in multi-GNSS. Remote Sens 10(1):80

Pan J, Hu X, Zhou S, Tang C, Guo R, Zhu L, Tang G, Hu G (2018) Time synchronization of new-generation BDS satellites using inter-satellite link measurements. Adv Space Res 61(1):145–153

Tang C, Hu X, Zhou S, Liu L, Pan J, Chen L, He F (2018) Initial results of centralized autonomous orbit determination of the new-generation BDS satellites with inter-satellite link measurements. J Geodesy 92(10):1155–1169

Teunissen PJG (1995) The least-squares ambiguity decorrelation adjustment: a method for fast GPS integer ambiguity estimation. J Geodesy 70:65–82

Wang N, Yuan Y, Li Z, Montenbruck O, Tan B (2016) Determination of differential code biases with multi-GNSS observations. J Geodesy 90(3):209–228

Wang C, Zhao Q, Guo J, Liu J, Chen G (2019a) The contribution of intersatellite links to BDS-3 orbit determination: model refinement and comparisons. Navigation 66(1):71–82

Wang N, Li Z, Montenbruck O, Tang C (2019b) Quality assessment of GPS, Galileo and BeiDou-2/3 satellite broadcast group delays. Adv Space Res 64(9):1764–1779

Wanninger L, Beer S (2015) BeiDou satellite-induced code pseudorange variations: diagnosis and therapy. GPS Solut 19(4):639–648

Wu Z, Zhou S, Hu X, Liu L, Shuai T, Xie Y, Tang C, Pan J, Zhu L, Chang Z (2018) Performance of the BDS3 experimental satellite passive hydrogen maser. GPS Solut 22(2):43

Xie X, Geng T, Zhao Q, Cai H, Zhang F, Wang X, Meng Y (2019) Precise orbit determination for BDS-3 satellites using satellite-ground and inter-satellite link observations. GPS Solut 23(2):40

Yang Y, Xu Y, Li J, Yang C (2018) Progress and performance evaluation of BeiDou global navigation satellite system: data analysis based on BDS-3 demonstration system. Sci China Earth Sci 61(5):614–624

Yang Y, Gao W, Guo S, Mao Y, Yang Y (2019) Introduction to BeiDou-3 navigation satellite system. Navigation 66(1):7–18

Zhang Y, Chen J, Zhou J, Yang S, Wang B, Chen Q, Gong X (2016) Analysis and application of BDS broadcast ephemeris bias. Acta Geod Cartogr Sin 45(S2):64–71

Zhang X, Wu M, Liu W, Li X, Yu S, Lu C, Wickert J (2017) Initial assessment of the COMPASS/BeiDou-3: new-generation navigation signals. J Geodesy 91(10):1225–1240

Zhang Y, Kubo N, Chen J, Wang J, Wang H (2019) Initial positioning assessment of BDS new satellites and new signals. Remote Sens 11(11):1320

Zhao L, Hu X, Zhou S, Tang C, Yang Y (2019) Primary exploration on approaches to establish BeiDou terrestrial reference frame. In: Proceedings of China satellite navigation conference. Lecture notes in electrical engineering 563, Springer, Singapore, pp 71–80. https://doi.org/10.1007/978-981-13-7759-4_7

Zhou S, Hu X, Liu L, Guo R, Zhu L, Chang Z, Tang C, Gong X, Li R, Yu Y (2016) Applications of two-way satellite time and frequency transfer in the BeiDou navigation satellite system. Sci China Phys Mech Astron 59(10):109511

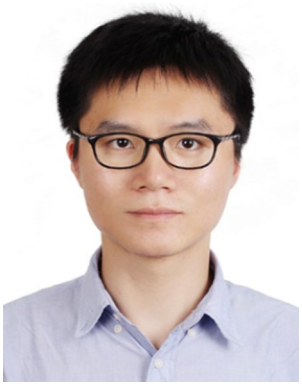

Yize Zhang is currently a postdoctoral researcher at the Tokyo University of Marine Science and Technology (TUMSAT). He received his Ph.D. degree from Tongji University in 2017. His current research mainly focuses on multi-GNSS precise positioning and GNSS biases analysis.

Nobuaki Kubo received his Master's degree in Electrical Engineering in 1998 from Hokkaido University. He received his doctorate in Engineering from the University of Tokyo in 2005. He resided at Stanford University in 2008 as a visiting scholar. He is now a professor at Tokyo University of Marine Science and Technology (TUMSAT), specializing in GPS/GNSS systems. His current interests are high-accuracy automobile navigation using RTK and multipath mitigation.

Junping Chen is the head of the GNSS data analysis group at Shanghai Astronomical Observatory (SHAO). He received his Ph.D. degree in Satellite Geodesy from Tongji University in 2007. Since 2011, he has been supported by the "one hundred talents" program of the Chinese Academy of Sciences. His research interests include multi-GNSS data analysis and GNSS augmentation systems.

Feng-Yu Chu is currently a visiting researcher at Tokyo University of Marine Science and Technology (TUMSAT). He received his Ph.D. degree from National Cheng Kung University in 2012. His main research interests include GNSS multiple-frequency data process, GPS precise positioning techniques, real-time kinematic positioning, phase ambiguity resolution, and the related applications in geodesy.

Ahao Wang is currently a Ph.D. candidate at the College of Surveying and Geo-Informatics, Tongji University, China. He has completed his B.S. at the School of Environment Science and Spatial Informatics in China University of Mining and Technology in 2015. His area of research focuses on the multi-GNSS PPP and its application in geoscience.

Jiexian Wang is currently a professor at Tongji University. He obtained his Ph.D. degree from Shanghai Astronomical Observatory (SHAO). His main research interest is in the study of GNSS positioning and its applications.